Interfering one-photon and two-photon ionization by femtosecond VUV pulses in the region of an intermediate resonance

Alexei N. Grum-Grzhimailo,[1,2,3] Elena V. Gryzlova,[1] Ekaterina I. Staroselskaya,[1,2] Joel Venzke,[4] and Klaus Bartschat[4]

[1]*Skobeltsyn Institute of Nuclear Physics, Lomonosov Moscow State University, Moscow 119991, Russia*

[2]*Faculty of Physics, Lomonosov Moscow State University, Moscow 119991, Russia*

[3]*Dipartimento di Fisica, Politecnico di Milano, Pizza Leonardo da Vinci 32, 20133 Milano, Italy*

[4]*Department of Physics and Astronomy, Drake University, Des Moines, Iowa 50311, USA*

(Received 3 May 2015; published 25 June 2015)

The electron angular distribution after atomic photoionization by the fundamental frequency and its second harmonic is analyzed for a case when the frequency of the fundamental scans the region of an intermediate atomic state. The angular distribution and its left-right asymmetry, due to the two-pathway interference between nonresonant one-photon and resonant two-photon ionization, sharply change as a function of the photon energy. The phenomenon is exemplified by both solving the time-dependent Schrödinger equation on a numerical space-time grid and by applying perturbation theory for ionization of the hydrogen atom in the region of the $1s$-$2p$ transition for femtosecond pulses as well as an infinitely long exposure to the radiation. Parametrizations for the asymmetry and the anisotropy coefficients, obtained within perturbation theory, reveal general characteristics of observable quantities as functions of the parameters of the radiation beam.

DOI: 10.1103/PhysRevA.91.063418 PACS number(s): 32.80.Rm, 32.80.Fb, 32.80.Qk, 32.90.+a

I. INTRODUCTION

Two-pathway interference is one of the key phenomena of quantum physics discussed in various aspects since the early days of quantum mechanics. The phenomenon manifests itself when the final state of a system can be reached by two independent paths from the same initial state. Then the probability to find the system in the final state is the squared magnitude of the sum of the transition amplitudes related to each of the paths. In addition to the absolute values of the amplitudes, this probability contains an interference term. Manipulating the two-pathway quantum interference is one of the practical methods to realize so-called "coherent control" of quantum phenomena [1–3], which is usually implemented by coherent light sources.

Two-pathway coherent control of photoionization and photodissociation has attracted much attention during the past two decades, from both experiment and theory alike. In studies controlling the total yield of the reaction products, which is one of the important goals of photochemistry, an ionization scheme employing the first and third harmonics ($\omega + 3\,\omega$) is appropriate, as well as other schemes with either both odd or both even numbers of photons participating in the two pathways (see, for example, Refs. [4–9]). On the other hand, interference between the absorption amplitudes for even and odd numbers of photons, e.g., in $\omega + 2\,\omega$ photoionization, does not contribute to the total yields. In this case, however, an effect appears in angle-resolved observations [10–12]. Coherent control via the two-pathway interference was reviewed, for example, in [3,13–15].

The recent commissioning of x-ray free-electron lasers (XFELs) and achievements in high-harmonic generation (HHG) have opened a new avenue in these investigations, extending them to the extreme ultraviolet (XUV) and x-ray wavelength regimes as well as femtosecond (fs) and attosecond (as) time domains. The present study was initially stimulated by the fact that radiation from XFELs usually contains a small fraction of the second harmonic. The latter is sometimes difficult to filter out, but it can strongly influence experimental data on the various parameters for two-photon ionization. Despite the relatively small intensity of the second harmonic, ionization by photons with frequency $2\,\omega$ (second harmonic, first-order process) may compete with, or even dominate, two-photon ionization by photons with frequency ω (fundamental, second-order process) [16], thereby causing uncertainty and potential ambiguity in the interpretation of the results. Consequently, it is important to study the interplay between the two ionization paths for particular experimental conditions. This interference may also be used to one's advantage in measuring the phase between the second harmonic and the fundamental. This is an important characteristic of an XFEL beam, but at the moment it can only be estimated by theoretical simulations of the laser pulse generation.

Consider atomic ionization processes in a linearly polarized bichromatic field, i.e., an electric field of the form

$$\mathcal{E}(t) = F(t)[\cos(\omega t + \phi_1) + \eta \cos(2\,\omega t + \phi_2)] \qquad (1)$$

with frequencies ω (fundamental radiation) and $2\,\omega$ (second harmonic). We take the same envelope function $F(t)$ for both the fundamental and the second harmonic, while the ratio of the amplitudes is specified by the real parameter η ($\eta > 0$). The corresponding carrier-envelope phases (CEPs) are denoted by ϕ_1 and ϕ_2, respectively. In making the dipole approximation, we neglect any spatial dependence of the field. Equation (1) implies that pulses of the fundamental and the second harmonic are not shifted in time, but potential effects of a time delay will also be briefly considered below.

Ionization by the field (1) from the same initial atomic state possesses interesting features due to the fact that the final states of the processes induced by the two field components are orthogonal: they lead to photoelectron partial waves with opposite parities. While interference between one-photon and two-photon ionization may be observed in the photoelectron angular distributions (PADs; see [11,12,17–19] and many more works), it vanishes in the angle-integrated cross section

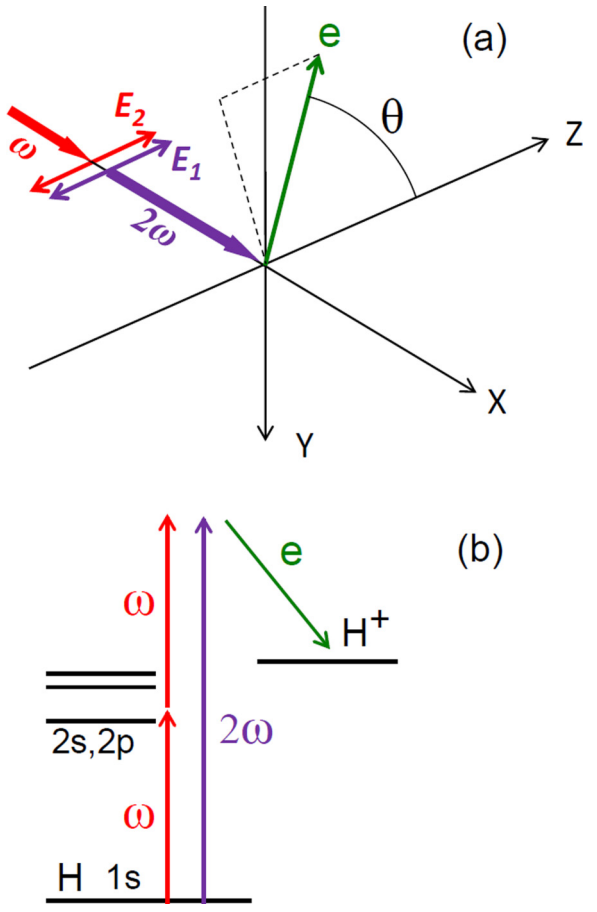

FIG. 1. (Color online) Geometry (a) and level scheme (b) of the $\omega + 2\,\omega$ process. The quantization (Z) axis is chosen along the linearly polarized laser field.

unless an external electric field is applied [20,21]. For a linearly polarized bichromatic radiation beam, the interference manifests itself in the asymmetry of the PAD with respect to the plane perpendicular to the electric field of the radiation; see Fig. 1(a). (We choose the Z axis of the coordinate system along the polarization direction.) The origin of this "left-right" asymmetry is a nonzero time-average cube of the electric field, $\langle \mathcal{E}^3 \rangle \neq 0$, while the time average of the field itself vanishes, i.e., $\langle \mathcal{E} \rangle = 0$ [22,23]. The asymmetry exhibits sinusoidal modulations as a function of the relative phase between the harmonics. Values as large as 4:1 for emission in opposite directions were observed in experiments [12] on photoionization of the Rb $5s\,^2S_{1/2}$ state.

It is important to note that the above considerations refer to the "multiphoton regime" of ionization, i.e., to comparatively weak fields with a Keldysh parameter $\gamma^2 = 2\,\omega^2 U/I \gg 1$ (here U is the ionization threshold and I is the peak intensity of the radiation in atomic units) and for pulses that contain many optical cycles. We assume that these conditions are fulfilled. Stronger fields and shorter pulses may lead to left-right asymmetries already for one-color ionization (see, for example, [24]).

An interesting open question concerns the potential effects of an intermediate state in the two-photon ionization path on the interference between the $\omega + 2\,\omega$ ionization ways, specifically to what extent such a state may influence the PADs. To our knowledge this discussion is currently still missing in the literature, although an intermediate resonance was used by Yin *et al.* [25] in their observation of two-path coherent control in a bound-free transition for the molecular NO system.

In the present paper we investigate this very point theoretically. We consider the prototype of photoionization of the hydrogen atom from its $1s$ ground state for photon energies near the excitation energy of the $2p$ state (0.375 a.u., corresponding to a wavelength of 121.6 nm), as shown schematically in Fig. 1(b). Studying atomic hydrogen avoids the difficulties associated with the description of a many-electron target and hence allows us to concentrate on the properties of the ionization process by the bichromatic field.

This paper is organized as follows. In the next section we present the theory of the PADs for $\omega + 2\,\omega$ ionization, considering the general aspects and concentrating on the formalism of perturbation theory applied to ionization of an s electron. Parametric formulas for the anisotropy parameters and asymmetry in the PADs are derived for the region of the intermediate state in the two-photon ionization branch. Section III presents numerical results for the hydrogen atom, which were obtained by direct numerical solution of the time-dependent Schrödinger equation (TDSE) and within nonstationary perturbation theory (PT). The results are analyzed and the possibility of performing a "complete experiment," in which all transition amplitudes are determined, is discussed. We finish with a brief summary.

II. THEORY

Within the dipole approximation and for an isotropic target, the PAD possesses axial symmetry about the polarization direction and is given by (for example, [26])

$$\frac{dW}{d\Omega} = \frac{W_0}{4\pi}\left[1 + \sum_{k=1}^{K} \beta_k P_k(\cos\theta)\right]. \tag{2}$$

Here θ is the electron emission direction with respect to the electric field of the linearly polarized radiation, while W_0 is the angle-integrated ionization probability. The β_k denote the anisotropy parameters, expressed in terms of the photoionization amplitudes. For one-photon ionization alone, only $k = 2$ contributes; for two-photon ionization $k = 2, 4$. Any asymmetry with respect to $\theta = 90^\circ$ is described by contributions from odd-rank Legendre polynomials, $P_k(\cos\theta)$ (k odd). For a combination of one-photon and two-photon ionization paths, specifically, contributions from $k = 1, 2, 3, 4$ should be accounted for. The odd polynomials appear due to coherent creation of photoelectron partial waves with opposite parities by the fundamental and the second harmonic of the radiation [12,18].

In order to quantify the interference in the PADs, we introduce the angle-differential asymmetry

$$A(\theta) = \frac{I(\theta) - I(180^\circ - \theta)}{I(\theta) + I(180^\circ - \theta)}, \tag{3}$$

where $I(\theta)$ is the intensity of the electron flux at the angle θ. In particular, $A(0^\circ)$ corresponds to the differential left-right asymmetry. It can be expressed in terms of the anisotropy

parameters β_k from Eq. (2) as

$$A(0^\circ) = \frac{\sum_{k=1,3,\ldots} \beta_k}{1 + \sum_{k=2,4,\ldots} \beta_k}. \tag{4}$$

The differential asymmetry is a function of the pulse parameters, such as the energy and intensity of the radiation, the envelope of the pulse, the relative contribution of the second harmonic, the carrier-envelope phases of the fundamental and the second harmonic, and the time delay between the fundamental and the second-harmonic pulses. The asymmetry (4), as well as the parameters β_k, generally vary within the photoelectron line.

In this paper we consider pulses (1) with a $\sin^2$ envelope, covering an integer number N ($N \gg 1$) of optical cycles: $F(t) = F_0 \sin^2 \Omega t$ ($\Omega = \omega/2N$, $0 \leqslant t \leqslant NT$) and $F(t) = 0$ otherwise. Here $T = 2\pi/\omega$ is the optical period while F_0 is the field amplitude of the first harmonic [cf. Eq. (1)]. For $N \gg 1$ only the relative phase $\phi = \phi_2 - \phi_1$ is essential in Eq. (1), but not the individual carrier-envelope phases ϕ_1 or ϕ_2. We set $\phi_1 = 0$ below.

We used two methods to calculate the photoelectron spectra and the asymmetry parameters β_k. In the first approach, we solved the TDSE as described in detail in [27]. The code was recently modified to run efficiently on parallel architectures such as those provided by modern supercomputers like STAMPEDE [28]. Starting from the $1s$ state of atomic hydrogen, we propagate the initial wave function in time to the end of the pulse ($t_{\rm end} = NT$) and then project the resulting wave packet on the stationary continuum states of the Coulomb field to find the partial-wave ionization amplitudes. The latter are combined to give the photoelectron spectrum and the anisotropy parameters β_k. The accuracy of the code has been checked many times over the years [29–31]. We are confident in the numerical correctness of its predictions, basically within the thickness of the lines for any of the physically significant parameters.

In the second method, the amplitudes were obtained within first-order and second-order time-dependent perturbation theory (PT). While the accuracy of the TDSE calculations for hydrogen are limited only by the numerics of the chosen space-time grid, the PT predictions are approximate already due to the original formulation. On the other hand, the calculation is much less laborious. The results should, of course, only be used within the domain of the PT's applicability. As we will illustrate below, they are particularly useful for analytically studying the dependence of the predictions on a wealth of laser parameters.

After ionization by a single photon of the second harmonic, the $1s$ bound electron becomes a p photoelectron, while it becomes either an s or d electron (via intermediate real or virtual p states) in two-photon absorption of the fundamental. In first and second order, the ionization amplitudes from the $1s$ state are expressed in terms of the matrix elements

$$\begin{aligned} U^{(1)} &\equiv \langle Ep \,|\, \hat{U}^{(1)} \,|\, 1s\rangle \\ &= -i \langle Ep|\hat{D}|1s\rangle \int_0^{NT} e^{i(E-E_{1s})t'} \mathcal{E}(t')dt' \\ &= -i D^{(1)}_{Ep,1s}\, T^{(1)} \end{aligned} \tag{5}$$

and

$$\begin{aligned} U^{(2)}_l &\equiv \langle El \,|\, \hat{U}^{(2)} \,|\, 1s\rangle \\ &= i^2 \sum\!\!\!\!\!\!\int_{E_n} \langle El \,|\, \hat{D} \,|\, E_n p\rangle \langle E_n p \,|\, \hat{D} \,|\, 1s\rangle \\ &\quad \times \int_0^{NT} e^{i(E-E_n)t'} \mathcal{E}(t') \int_0^{t'} e^{i(E_n - E_{1s})t''} \mathcal{E}(t'')dt''dt' \\ &= -\sum\!\!\!\!\!\!\int_{E_n} D^{(2)}_{El,1s}(E_n)\, T^{(2)}_{E_n} \qquad (l = 0, 2), \end{aligned} \tag{6}$$

respectively. The time dependence is only contained here in the factors $T^{(1)}(t)$ and $T^{(2)}_{E_n}(t)$, while the radial dipole matrix elements in (5) and (6) are given by

$$D^{(1)}_{Ep,1s} = i\, e^{-i\varphi_p} \frac{1}{\sqrt{3}} \int_0^\infty P_{Ep}(r) r\, P_{1s}(r) dr \tag{7}$$

and (for linearly polarized radiation)

$$\begin{aligned} D^{(2)}_{El,1s}(E_n) = i^l\, e^{-i\varphi_l} &\frac{1}{\sqrt{2l+1}} (10, 10 \,|\, l0)^2 \\ &\times \int_0^\infty P_{El}(r) r\, P_{E_n p}(r) dr \\ &\times \int_0^\infty P_{E_n p}(r) r\, P_{1s}(r) dr. \end{aligned} \tag{8}$$

Here $P_{1s}(r)$ and $P_{E_n p}(r)$ are the radial electron functions of the ground state $1s$ and the intermediate states $E_n p$ with the energy E_n, respectively; $P_{El}(r)$ and φ_l are the Coulomb function and the Coulomb phase of the continuum electron with the orbital momentum l and energy E; $(j_1 m_1, j_2 m_2 \,|\, jm)$ is a Clebsch-Gordan coefficient. The matrix elements (7) and (8) are smooth functions of the photoelectron energy.

The time-dependent factor in Eq. (5) is of the form

$$T^{(1)} = F_0 \int_0^{NT} \sin^2(\Omega t') \cos(2\,\omega t' + \phi) e^{i(E-E_{1s})t'} dt'. \tag{9}$$

In the rotating-wave approximation, which is well satisfied when $N \gg 1$, the phase ϕ in Eq. (9) can be decoupled and just becomes a factor $e^{-i\phi}$.

The time-dependent factor of the second-order amplitude (6) is of the form

$$\begin{aligned} T^{(2)}_{E_n} = F_0^2 &\int_0^{NT} \sin^2(\Omega t') \cos(\omega t') e^{i(E-E_n)t'} \\ &\times \int_0^{t'} \sin^2(\Omega t'') \cos(\omega t'') e^{i(E_n - E_{1s})t''} dt''dt'. \end{aligned} \tag{10}$$

Using standard techniques (see, for example, [32]), one obtains the following expressions for the anisotropy parameters:

$$\beta_2 = 2W_0^{-1}\left[\sqrt{5}\,\mathrm{Re}\big(U^{(2)}_d\, U^{(2)*}_s\big) + \eta^2 |U^{(1)}|^2 + \frac{5}{7}\big|U^{(2)}_d\big|^2\right], \tag{11}$$

$$\beta_4 = \frac{18}{7} W_0^{-1} \big|U^{(2)}_d\big|^2, \tag{12}$$

$$\beta_1 = 2\sqrt{3}\,\eta\, W_0^{-1}\mathrm{Re}\left[\left(U_s^{(2)} + \frac{2}{\sqrt{5}}U_d^{(2)}\right)U^{(1)*}\right], \quad (13)$$

$$\beta_3 = 6\sqrt{\frac{3}{5}}\,\eta\, W_0^{-1}\,\mathrm{Re}\left(U_d^{(2)}\,U^{(1)*}\right). \quad (14)$$

Here

$$W_0 = \eta^2|U^{(1)}|^2 + \left|U_s^{(2)}\right|^2 + \left|U_d^{(2)}\right|^2 \quad (15)$$

and Re[X] denotes the real part of the complex quantity X. Substituting Eqs. (11)–(15) into Eq. (4), we obtain

$$A(0^\circ) = \frac{\beta_1+\beta_3}{1+\beta_2+\beta_4} = \frac{2\sqrt{3}\,\eta\,\mathrm{Re}\left[\left(U_s^{(2)}+\sqrt{5}\,U_d^{(2)}\right)U^{(1)*}\right]}{3\,\eta^2|U^{(1)}|^2 + \left|U_s^{(2)}+\sqrt{5}\,U_d^{(2)}\right|^2}. \quad (16)$$

Finally, the (dimensionless) probability for ionizing the hydrogen atom during the entire pulse is $\int W_0\,dE$.

When evaluating $U_l^{(2)}$ numerically according to Eqs. (6), (8), and (10), we included nine intermediate discrete $E_n p$ states ($n = 2, 3, \ldots, 10$) in Eq. (6). Further increasing the number of intermediate states to 15 did not change the predicted anisotropy parameters for photon energies in the region of the $1s$-$2p$ transition within the thickness of the lines.

Finally, we applied perturbation theory with infinitely long "pulses" of constant amplitude F_0'. To calculate the corresponding matrix elements, we assumed an adiabatic switch-on/off of the field. Taking afterwards the integrals over time in Eqs. (9) and (10), and considering the limit $NT \to \infty$, we obtain the ionization rate

$$\frac{dW}{dt} = 2\pi\, W_0\,\delta(E - E_{1s} - 2\omega), \quad (17)$$

where $U^{(1)}$ and $U_l^{(2)}$ are reduced to

$$U^{(1)} = i\frac{F_0'}{2}e^{-i\phi}D^{(1)}_{Ep,1s}, \quad (18)$$

$$U_l^{(2)} = i\frac{F_0'^2}{4}\sum\!\!\!\!\!\!\int_{E_n} \frac{D^{(2)}_{El,1s}(E_n)}{E_n - E_{1s} - \omega + i0}. \quad (19)$$

Note that we omitted here some terms that are negligible in our spectral region of interest. To calculate the second-order amplitude (19) we applied the variationally stable procedure [33–35] with the same set of Slater orbitals used in [34] for two-photon ionization. As a check, we reproduced the exact analytical [36] partial cross sections and angular anisotropy parameters for two-photon ionization of atomic hydrogen with an accuracy of four significant digits. We intend to use this approach also in our future studies with many-electron targets, where the exact electron wave functions are not known.

When taking the limit $NT \to \infty$ one should be careful regarding the mutual normalization of the first-order and second-order amplitudes, which depend on the intensity of the incident radiation beam through different powers of F_0. To normalize the amplitudes to the same number of incoming photons, we impose the condition

$$\int_0^{NT}[F(t)\cos\omega t]^2\,dt = \int_0^{NT}(F_0'\cos\omega t)^2\,dt. \quad (20)$$

This yields the following relationship between the field amplitudes: $F_0' = \sqrt{3/8}F_0$.

Equations (16)–(19) can be used to show that, within the model just containing the single $2p$ intermediate state, the left-right asymmetry for the infinite pulse takes the remarkably simple parametric form

$$A(0^\circ) = \frac{2\varepsilon}{\varepsilon^2+1}\cos(\phi+\phi_0), \quad (21)$$

where

$$\varepsilon = \frac{\Delta\omega}{\frac{1}{2}\Gamma_\omega}, \quad (22)$$

$$\Gamma_\omega = \frac{F_0'}{\sqrt{3}\eta}\left|\frac{D_s^{(2)}+\sqrt{5}D_d^{(2)}}{D^{(1)}}\right|, \quad (23)$$

$$\phi_0 = \arg\left[\left(D_s^{(2)}+\sqrt{5}D_d^{(2)}\right)D^{(1)*}\right]. \quad (24)$$

Here $\Delta\omega = \omega - (E_{2p} - E_{1s})$, $E_r = 2E_{2p} - E_{1s}$ is the photoelectron energy in the resonance ($E_r = 0.250$ a.u.), and we abbreviated $D_s^{(2)} = D^{(2)}_{E_r s,1s}(E_{2p})$, $D_d^{(2)} = D^{(2)}_{E_r d,1s}(E_{2p})$, and $D^{(1)} = D^{(1)}_{E_r p,1s}$, respectively. The values of $D_s^{(2)}$, $D_d^{(2)}$, and $D^{(1)}$ are constants.

The anisotropy parameters (11)–(14) for the infinite pulse may also be reduced to simple parametric forms:

$$\beta_2 = 2\left(1 - \frac{B_2}{\epsilon^2+1}\right), \quad (25)$$

$$\beta_4 = \frac{B_4}{\epsilon^2+1}, \quad (26)$$

$$\beta_1 = \frac{B_1\,\epsilon}{\epsilon^2+1}\cos(\phi+\phi_1), \quad (27)$$

$$\beta_3 = \frac{B_3\,\epsilon}{\epsilon^2+1}\cos(\phi+\phi_3), \quad (28)$$

where

$$\epsilon = \frac{\Delta\omega}{\frac{1}{2}\Gamma_\beta}, \quad (29)$$

$$\Gamma_\beta = \frac{F_0'}{\eta}\sqrt{\frac{\left|D_s^{(2)}\right|^2 + \left|D_d^{(2)}\right|^2}{|D^{(1)}|^2}}, \quad (30)$$

$$B_2 = C^{-1}\left[\frac{2}{7}\left|D_d^{(2)}\right|^2 + \left|D_s^{(2)}\right|^2 - \sqrt{5}\mathrm{Re}\left(D_d^{(2)}D_s^{(2)*}\right)\right], \quad (31)$$

$$B_4 = \frac{18}{7}C^{-1}\left|D_d^{(2)}\right|^2, \quad (32)$$

$$B_1 = -2\sqrt{3}C^{-\frac{1}{2}}\left|D_s^{(2)} + \frac{2}{\sqrt{5}}D_d^{(2)}\right|, \quad (33)$$

$$B_3 = -\frac{6\sqrt{3}}{\sqrt{5}} C^{-\frac{1}{2}} \left| D_d^{(2)} \right|, \tag{34}$$

$$\phi_1 = \arg\left[\left(D_s^{(2)} + \frac{2}{\sqrt{5}} D_d^{(2)} \right) D^{(1)*} \right], \tag{35}$$

$$\phi_3 = \arg\left(D_d^{(2)} D^{(1)*} \right), \tag{36}$$

$$C = \left| D_s^{(2)} \right|^2 + \left| D_d^{(2)} \right|^2. \tag{37}$$

Although Eqs. (21)–(37) are only valid in a restricted domain of pulse parameters, these analytical results provide a foundation for the qualitative understanding of the features associated with $\omega + 2\omega$ ionization in the vicinity of an intermediate resonance.

Within the above model, the width of the resonant structure Γ_ω (23) in the left-right asymmetry and the width Γ_β (30), which is the same for all anisotropy parameters β_k ($k = 1, 2, 3, 4$), are independent of the relative phase of the harmonics ϕ and of the interference between the first-order and second-order ionization amplitudes. The latter interference only enters through the phase offsets ϕ_0, ϕ_1, and ϕ_3. The widths Γ_ω and Γ_β increase linearly with the amplitude of the electric field and are inversely proportional to η. Some useful relations between the parameters are

$$B_3^2 = \frac{42}{5} B_4, \tag{38}$$

$$\left(\frac{B_1}{B_3} \right)^2 = \frac{2(4B_2 - 9)}{17 B_4} - \frac{3}{7}, \tag{39}$$

$$\phi_0 = \phi_1 + \frac{3}{\sqrt{5}} \phi_3, \tag{40}$$

$$\left(\frac{\Gamma_\omega}{\Gamma_\beta} \right)^2 = 1 + \frac{1}{3}(2B_2 + B_4). \tag{41}$$

These, and others, may help in determining different dynamical parameters of the process.

III. RESULTS AND DISCUSSION

Detailed calculations solving the TDSE were performed for pulses with peak intensities of 10^{12} W/cm^2 and 10^{13} W/cm^2 for $N = 40$. The latter corresponds to an entire pulse duration of approximately 17 fs (or a FWHM of the intensity of 6 fs). For different photon frequencies the pulse durations change slightly, but this is not important in our analysis within a narrow range near the resonant $1s$-$2p$ transition.

For the cases considered in the present work, the electric field strength is much weaker than an atomic unit and, moreover, the Keldysh parameter $\gamma \gg 1$ indicates that the multiphoton regime of ionization is realized. At the same time, since the photon frequency is near the $1s$-$2p$ resonance, the applicability of the lowest-order perturbation theory is questionable. To analyze this in more detail, we present in Fig. 2 the population of the excited $2p$ state as function of time calculated in the TDSE approach for 40-cycle pulses with different peak intensities and two carrier frequencies: on-resonance and slightly off-resonance. Recall that the principal

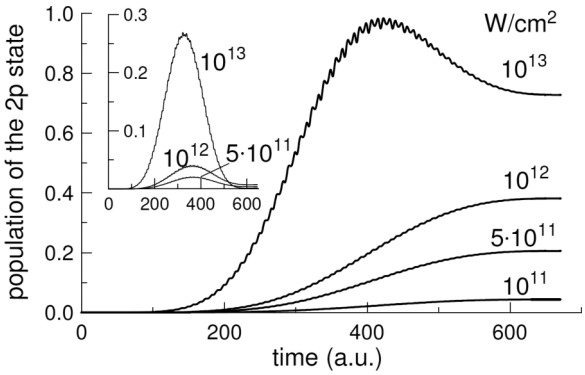

FIG. 2. TDSE results for the population of the H($2p$) state as function of time for different peak intensities (indicated near the curves) and $N = 40$. Main plot: resonance carrier frequency ($\omega = 0.375$ a.u.); inset: wing of the resonance ($\omega = 0.390$ a.u.).

condition for the applicability of PT is a small population probability of all target states except for the initial state. For the pulses in this study, the atoms are predominantly distributed between the ground $1s$ and the excited $2p$ states, while all other atomic states are negligibly populated. At the resonant energy, for example, the total ionization probability reaches only 0.0004 and 0.01 for pulses with $N = 40$ at intensities of $I = 10^{12}$ W/cm^2 and $I = 10^{13}$ W/cm^2, respectively. The corresponding populations of the $2s$ state, which can be reached by a two-photon 2ω-ω transition via the continuum, are less than 0.0004 and 0.02, respectively.

It is clear from Fig. 2 that PT should fail for the relatively high peak intensity of 10^{13} W/cm^2, while it should be appropriate for the low peak intensity of 10^{11} W/cm^2. At intermediate intensities of 5×10^{11} W/cm^2 and 10^{12} W/cm^2, PT might work qualitatively close to the resonance photon energy but much better on the wings of the resonance. The Rabi period of the $1s$-$2p$ transition for the *monochromatic* radiation with an intensity of 10^{13} W/cm^2 is 500 a.u. The population of the $2p$ state, therefore, oscillates with a period of 250 a.u. This explains why we already see part of a Rabi oscillation in the corresponding curve in Fig. 2. The figure also illustrates the transition to the adiabatic regime of excitation of the $2p$ state for larger detuning. In that case the $2p$ population follows the pulse envelope (see the inset).

Figure 3(a) shows contributions from ionization by the fundamental with peak intensities of 10^{12} W/cm^2 and 10^{13} W/cm^2 and its second harmonic as a function of the photon energy in the region of the H $1s \rightarrow 2p$ excitation. The curves in Fig. 3(a) present the ionization probability $P = \int P(E)\, dE$, where $P(E)$ is the probability density of the ionization as function of the photoelectron energy and the integral is taken over the main photoelectron line. The value of $\eta = 0.225$ in these calculations corresponds to 5% of the second-harmonic intensity relative to the intensity of the fundamental. For this value of η, the intensity of the main photoelectron line generated by the fundamental and that of the second harmonic are practically equal for $I = 10^{12}$ W/cm^2 at the resonance energy. This provides a good opportunity to reveal the effects of the intermediate state, since one can expect the maximum interference effect in the PAD for photon energies near the resonance.

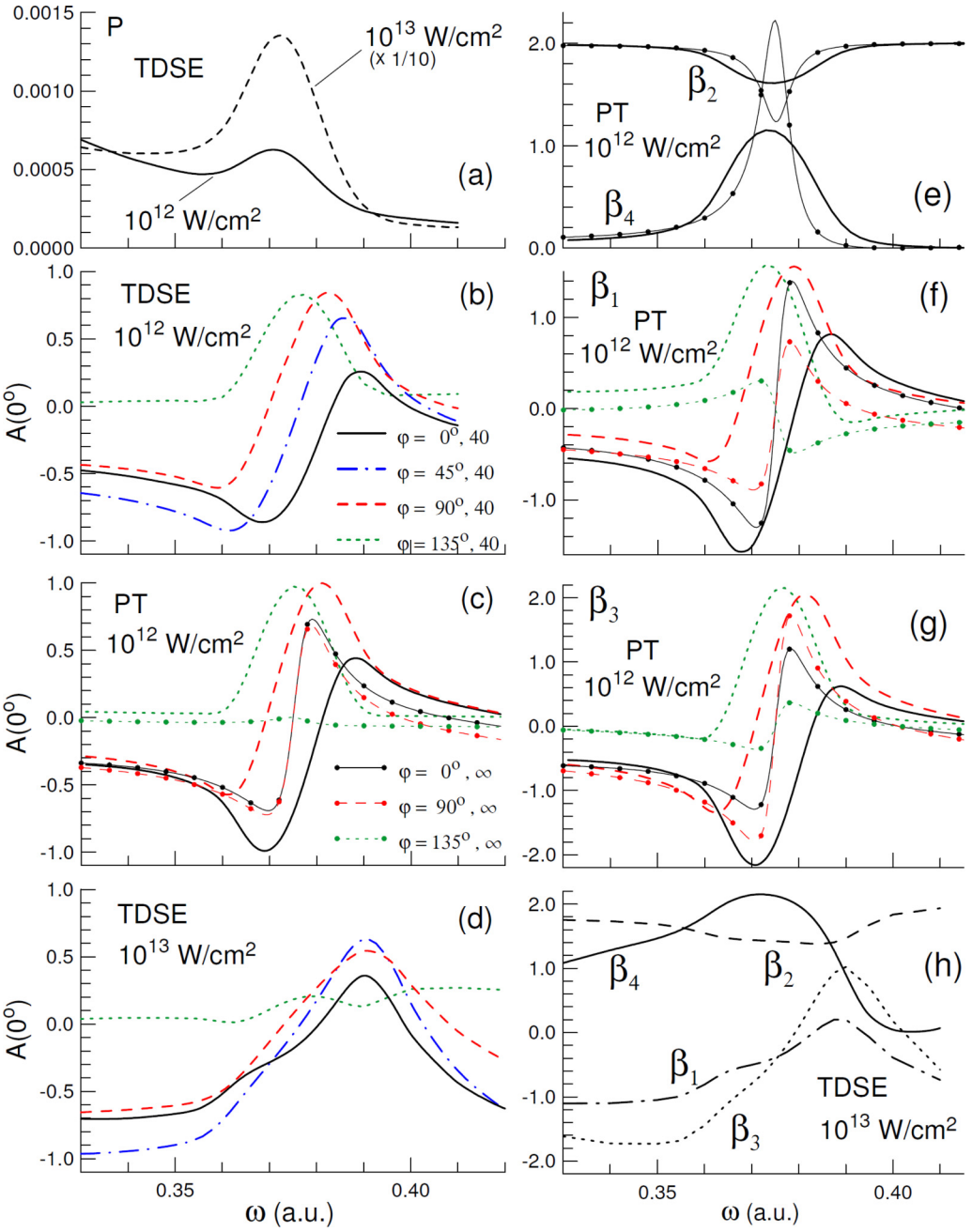

FIG. 3. (Color online) Theoretical results for $\eta = 0.225$. (a) Ionization probability integrated over the main photoelectron line (see text for details) as a function of the photon energy, TDSE ($N = 40$). Left-right asymmetry $A(0^\circ)$ and anisotropy parameters β_k, averaged over the main photoelectron line, as a function of the photon energy for different relative phases between the fundamental and the second harmonic: (b) $A(0^\circ)$, 10^{12} W/cm^2, TDSE ($N = 40$); (c) $A(0^\circ)$, 10^{12} W/cm^2, PT ($N = 40$ and infinite pulse); (d) $A(0^\circ)$, 10^{13} W/cm^2, TDSE ($N = 40$); (e) β_2, β_4, 10^{12} W/cm^2, PT ($N = 40$ and infinite pulse); (f) β_1, 10^{12} W/cm^2, PT ($N = 40$ and infinite pulse), $\phi = 0^\circ, 90^\circ, 135^\circ$; (g) same as (f) for β_3; (h) β_1, β_2, β_3, β_4, 10^{13} W/cm^2, TDSE ($N = 40$), $\phi = 0^\circ$. The dotted curves in the PT panels are for the infinite pulse. In panels (b), (c), (d), (f), and (g), a common notation for the curves is adopted.

In the angle-integrated photoelectron spectra [see Fig. 3(a)], contributions from the fundamental and the second harmonic are incoherent, since the interference terms vanish. For photon energies away from the resonance the two-photon contribution quickly drops. For $I = 10^{13}$ W/cm^2, PT up to second order (not even shown) fails completely. This is expected, since the relative probability of two-photon ionization with respect to one-photon ionization should increase in PT by a factor of 100 when the intensity is increased by a factor of 10. This is much larger than the TDSE predictions presented in Fig. 3(a).

Figures 3(e)–3(h) show the anisotropy parameters, which are averaged over the main photoelectron line, $\beta_k = P^{-1} \int \beta_k(E)\, P(E)\, dE$, and Figs. 3(b)–3(d) show the left-right asymmetry calculated with the averaged parameters β_k. Sharp variations of the anisotropy parameters β_k in the PADs (2) and the left-right asymmetry (3) when scanning the photon energy ω through the resonance are exhibited

in Figs. 3(b)–3(h) for four values of the relative phase ϕ between the harmonics. Since changing ϕ by 180° leads to a sign reversal of the asymmetry, we only present curves for $\phi \leqslant 180°$ ($\phi = 0°, 45°, 90°, 135°$). For arbitrary but fixed ω, the asymmetry, as well as the anisotropy parameters β_k for odd k, vanish after averaging over ϕ in the interval $0 \leqslant \phi \leqslant 360°$.

The asymmetries $A(0°)$ obtained for similar pulses in the TDSE and PT calculations for 10^{12} W/cm^2 are close to each other [see Figs. 3(b) and 3(c)]. This allows us to use the PT results for this intensity to reveal the main features of the PADs as a function of such parameters as ω, η, ϕ, and N. Such an endeavor would be very laborious by solving the TDSE for all the cases.

In the perturbative regime, the left-right asymmetry exhibited in Figs. 3(b) and 3(c) and the anisotropy parameters in the PAD shown in Figs. 3(e)–3(g) exhibit Fano-like profiles as function of the photon energy. For the infinite pulse within PT and an isolated resonance, it follows from Eqs. (21), (27), and (28) that $A(0°)$, β_1, and β_3 cross zero at the resonant photon energy ($\varepsilon = \epsilon = 0$), independent of the relative phase ϕ between the harmonics and the values of the dipole matrix elements. This is confirmed by numerical calculations according to Eqs. (11)–(16) for the infinite pulse [see Figs. 3(c), 3(f), and 3(g)]. Contributions from other intermediate states do not noticeably shift the values of $A(0°)$, β_1, and β_3 from zero at the resonant photon energy. As the photon energy deviates from the resonance, contributions from other intermediate states are no longer negligible. As seen in Figs. 3(c), 3(f), and 3(g), this contribution causes nonzero values of $A(0°)$, β_1, and β_3 far from the resonance. This is in contradiction with the simple forms given by Eqs. (21), (27), and (28). The sign of the above three parameters depends on the sign of $\cos(\phi + \phi_k)$ ($k = 0, 1, 3$) and, consequently, on the interference between the first-order and second-order ionization amplitudes at the resonance photoelectron energy E_r, as well as on the relative phase ϕ between the first and the second harmonics.

Only four curves are presented in Fig. 3(e), because in the perturbative regime the anisotropy parameters β_2 [see Eqs. (11) and (25)] and β_4 [see Eqs. (12) and (26)] are independent of the relative phase ϕ between the harmonics. (Small variations of β_2 and β_4 with ϕ, due to deviations from the rotating-wave approximation, are not seen in the figure.) According to Eqs. (25) and (26), the resonances in β_2 and β_4 for the infinite pulse are symmetric with respect to the resonance photon energy. The asymmetry in the corresponding curves shown in Fig. 3(e) is related to contributions to the two-photon amplitude from other intermediate states (including the continuum) [37,38]. The latter are taken into account in our numerical calculation.

For the pulse of finite time duration, the profiles of the left-right asymmetry as a function of the photon energy become broader and can also change the shape substantially. Furthermore, the zero of the left-right asymmetry on the energy scale is shifted differently depending on the relative phase ϕ between the harmonics. Such examples are presented in Fig. 3(c). The TDSE calculations also illustrate that a further broadening of the resonance structure occurs with increasing intensity [Fig. 3(d)] in the domain where PT is already not appropriate.

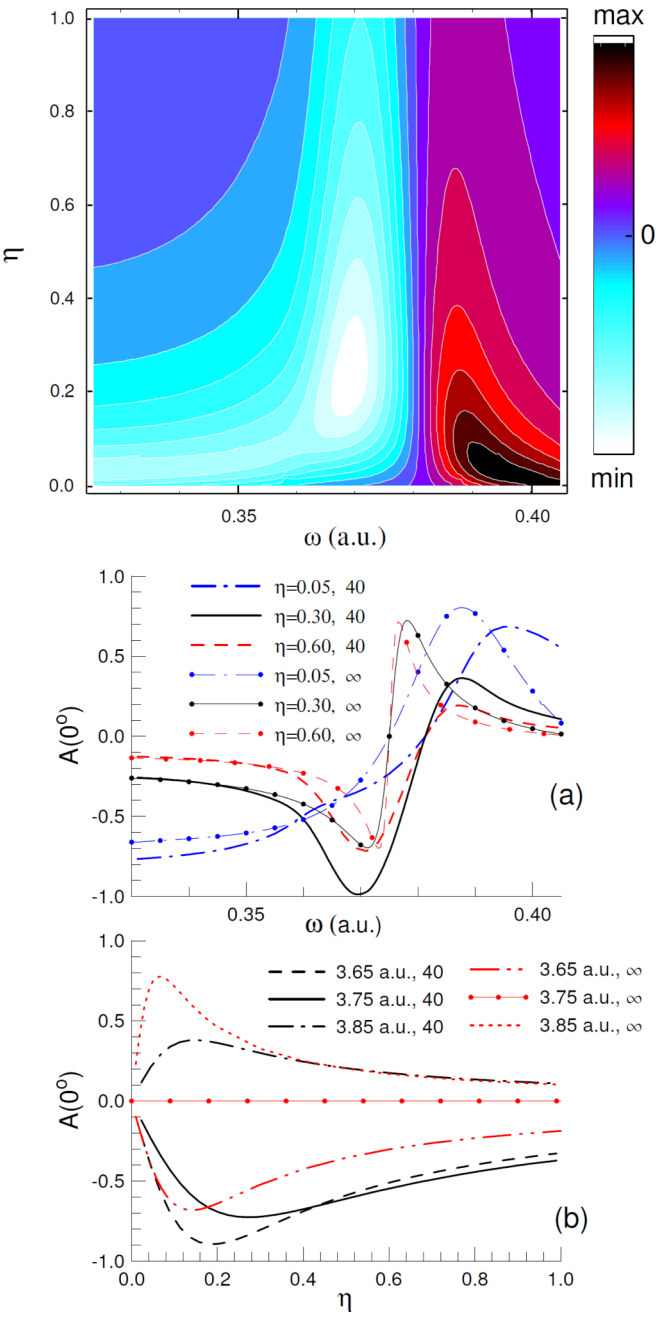

FIG. 4. (Color online) Left-right asymmetry $A(0°)$, averaged over the main photoelectron line, as obtained in PT for 10^{12} W/cm^2 as a function of the photon energy and relative contribution of the second harmonic for $\phi = 0°$. The contour plot is for $N = 40$; cuts along the ω (a) and η (b) axes are compared to results for an infinite (∞) pulse.

Figure 4 presents the left-right asymmetry as a function of the photon energy and the relative intensity ($0 \leqslant \eta \leqslant 1$) of the second harmonic. The results for the contour plot (upper panel) were obtained by PT calculations for $I = 10^{12}$ W/cm^2 with $N = 40$ and $\phi = 0°$. They are compared with the results for the infinite pulse on the cuts of the contour plot along the axis of the photon energy ω and the parameter η in Figs. 4(a) and 4(b), respectively.

To understand the general tendencies in the left-right asymmetry seen in Fig. 4, we rewrite Eq. (21) in the form

$$A(0^\circ) = \frac{2\tilde{\eta}}{\tilde{\eta}^2+1}\cos(\phi+\phi_0), \tag{42}$$

$$\tilde{\eta} = \frac{\eta}{\frac{1}{2}\Gamma_\eta}, \tag{43}$$

$$\Gamma_\eta = \frac{F_0'}{\sqrt{3}|\Delta\omega|}\left|\frac{D_s^{(2)}+\sqrt{5}D_d^{(2)}}{D^{(1)}}\right|, \tag{44}$$

where the phase offset ϕ_0 is defined by Eq. (24). The (approximate) inverse proportionality of the widths Γ_ω and Γ_η to η and $\Delta\omega$, respectively [see Eqs. (23) and (44) for infinite pulses], is very well seen in the contour plot as a hyperbolic area. The asymmetry $A(0^\circ)$ does not change sign as function of η ($\eta \geqslant 0$). It starts from zero at $\eta = 0$, and after reaching a maximum it approaches zero again when $\eta \to \infty$. These results make sense, since the two limiting cases correspond to pure one-photon and two-photon ionization, respectively, i.e., to cases for which the parity of the photoelectron wave function is well defined. This tendency is clearly visible in Fig. 4(b). Our calculations also reveal that the details of the behavior of $A(0^\circ)$ depend on the pulse duration. For the resonance value $\omega_r = 0.375$ a.u. and an infinite pulse, two-photon resonant ionization so strongly dominates one-photon ionization that the left-right asymmetry vanishes [Fig. 4(b)], independently of the value of η in the interval considered. For the finite pulse with carrier frequency ω_r, its spectrum covers the interval around ω_r. Here one-photon ionization starts to contribute significantly and the asymmetry acquires large magnitudes, with the details depending on the value of η.

Figure 5 illustrates a strong ϕ-dependence of the parameters β_k in the PAD (2) for odd k and of asymmetry $A(0^\circ)$ for the resonant photon energy of 0.375 a.u. Note that all parameters β_k for $k > 4$, appearing in the TDSE calculations, are negligible. For even k the parameters β_k are independent of the interference between the one-photon and two-photon ionization channel and, therefore, are also independent of ϕ.

The asymmetry generally decreases with increasing time delay τ between the fundamental and second-harmonic pulses. It vanishes when the pulses do not overlap in time (see the inset in Fig. 5). The ϕ-dependence of the type seen in Eqs. (21) and (42) is valid for the left-right asymmetry and the parameters β_k (k odd) within PT for pulses with finite time duration, but the phase offsets are different and depend on the pulse parameters. Although the asymmetry $A(0^\circ)$ calculated by either solving the TDSE or in PT ($N = 40$) for $I = 10^{12}$ W/cm^2 differ only slightly, the TDSE and PT curves for the β_k parameters may deviate more strongly from each other (e.g., β_1 in Fig. 5). This is the consequence of the PT no longer being quantitatively valid for $I = 10^{12}$ W/cm^2.

An interesting point concerns the information that can be extracted from the various parameters measured in $\omega + 2\omega$ ionization. This depends, of course, on which parameters of the radiation beam are known and controlled. When the relative phase ϕ between the fundamental and the second harmonic is known, the relative phases between the one-photon s-p and two-photon s-s, s-d amplitudes can be measured [17,39],

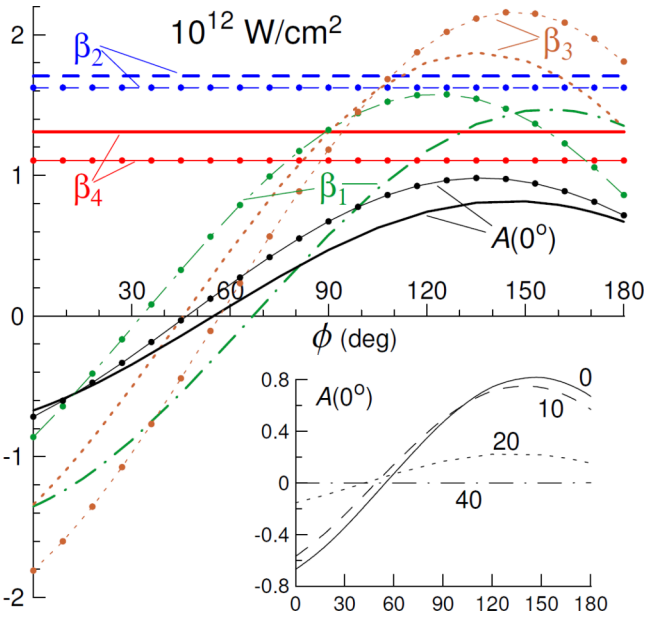

FIG. 5. (Color online) Asymmetry parameters β_k and asymmetry $A(0^\circ)$ for the resonance photon energy of 0.375 a.u. and $\eta = 0.225$ as a function of the relative phase between the harmonics ($N = 40$, 10^{12} W/cm^2). The results were calculated in PT (curves with dots) and by solving the TDSE (curves without dots). The parameters are averaged over the photoelectron line. The inset shows the asymmetry $A(0^\circ)$ for different time delays τ between the fundamental and the second harmonic pulses, calculated by solving the TDSE. Value of τ measured in multiples of optical cycles is indicated for each curve.

provided perturbation theory can be employed in the theoretical treatment of one-photon and two-photon ionization, and lasers with appropriate (circular/linear) polarizations are used.

Turning to XFELs, where the phase and polarization control of the radiation beam is much more difficult than with optical lasers, let us consider linearly polarized radiation with an unknown (but fixed within a narrow photon energy interval) relative phase ϕ between the harmonics. Suppose $A(0^\circ)$, β_1, β_2, β_3, and β_4 can be measured as functions of the photon energy in the region of an isolated $2p$ resonance at low intensity ($\approx 10^{11}$ W/cm^2), when PT can be applied and the pulse is long enough to use Eqs. (21)–(41). Then a recipe to measure the phase ϕ between the fundamental and the second harmonic could look as follows. The strategy is to find $\cos(\phi+\phi_0)$, $\cos(\phi+\phi_1)$, and $\cos(\phi+\phi_3)$ (i.e., $\phi+\phi_0$, $\phi+\phi_1$, $\phi+\phi_3$ except for the signs) from the experimental data and then use Eq. (40) to extract ϕ. The value of $\cos(\phi+\phi_0)$ follows directly from the measurement of $A(0^\circ)$ according to Eq. (21). The products $B_1\cos(\phi+\phi_1)$ and $B_3\cos(\phi+\phi_3)$ follow from the measurements of β_1 (27) and β_3 (28), respectively. The value of β_4 (26) gives B_4 and, hence, B_3 via Eq. (38). Finally, the photon-energy dependence of $A(0^\circ)$ and β_k yields the ratio (41). This gives us additionally the parameters B_2 and B_1 via Eq. (39). Note that the results of this procedure, within the model, are independent of the pulse intensity and the relative contribution of the second harmonic η. Having the above information, one can find the relative phase ϕ and also the ratio of the amplitudes $D_s^{(2)}$ and $D_d^{(2)}$ of the two channels for two-photon ionization, as well as the ratio of

the one-photon and two-photon amplitudes. This constitutes a "complete experiment" within the parametrization used to describe the process [40].

IV. SUMMARY

Keeping in mind applications to photoprocesses with XFELs, we theoretically studied interference effects in two-pathway ionization by the fundamental (two-photon ionization) and its second harmonic (one-photon ionization) near an intermediate atomic resonance. As a prototype example, ionization from the $1s$ ground state of the hydrogen atom was analyzed in the vicinity of the $1s$-$2p$ transition. Within perturbation theory, parametrizations were derived for the anisotropy parameters in the photoelectron angular distribution and for the left-right asymmetry in the region of the isolated intermediate resonance. General features of these observable quantities were revealed as functions of the photon energy, the relative contribution of the second harmonic, and the relative phase between the fundamental and its second harmonic. Particular prescriptions were formulated regarding the extraction of the maximal dynamical information on the photoionization process via photoelectron angular distributions in tight control of the XFEL beam parameters.

ACKNOWLEDGMENTS

A.N.G. gratefully acknowledges the hospitality of Politecnico di Milano and financial support of the Italian Ministry of Research (Project FIRB No. RBID08CRXK). The authors benefited greatly from stimulating discussions with Giuseppe Sansone, Kevin Prince, and Kiyoshi Ueda. The work of J.V. and K.B. was supported by the United States National Science Foundation under Grant No. PHY-1430245 and XSEDE Allocation No. PHY-090031.

[1] M. Shapiro and P. Brumer, J. Chem. Phys. **84**, 4103 (1986).
[2] P. Brumer and M. Shapiro, *Principles of the Quantum Control of Molecular Processes* (Wiley-VCH, Berlin, 2003).
[3] C. Brif, R. Chakrabati, and H. Rabitz, New J. Phys. **12**, 075008 (2010).
[4] M. Shapiro, J. W. Hupburn, and P. Brumer, Chem. Phys. Lett. **149**, 451 (1988).
[5] C. Chen, Y. Y. Yin, and D. S. Elliott, Phys. Rev. Lett. **64**, 507 (1990).
[6] V. D. Kleiman, L. Zhu, X. Li, and R. J. Gordon, J. Chem. Phys. **102**, 5863 (1995).
[7] G. Xing, X. Wang, X. Huang, R. Bersohn, and B. Katz, J. Chem. Phys. **104**, 826 (1996).
[8] X. Wang, R. Bersohn, K. Takahashi, K. Kawasaki, and H. L. Kim, J. Chem. Phys. **105**, 2992 (1996).
[9] S. Lee, J. Chem. Phys. **108**, 3903 (1998).
[10] K. J. Schafer and K. C. Kulander, Phys. Rev. A **45**, 8026 (1992).
[11] N. B. Baranova, I. M. Beterov, B. Ya. Zel'dovich, I. I. Ryabtsev, A. N. Chudinov, and A. A. Shul'ginov, Pis'ma Zh. Eksp. Teor. Fiz. **55**, 431 (1992) [JETP Lett. **55**, 439 (1992)].
[12] Y.-Y. Yin, C. Chen, D. S. Elliott, and A. V. Smith, Phys. Rev. Lett. **69**, 2353 (1992).
[13] M. Shapiro and P. Brumer, in *Advances in Atomic, Molecular, and Optical Physics*, edited by B. Bederson and H. Walther, Vol. 42 (Academic Press, San Diego, 2000), p. 287.
[14] E. Ehlotzky, Phys. Rep. **345**, 175 (2001).
[15] V. A. Astapenko, Quantum Electron. **36**, 1131 (2006).
[16] L. A. A. Nikolopoulos and P. Lambropoulos, Phys. Rev. A **74**, 063410 (2006).
[17] Z.-M. Wang and D. S. Elliott, Phys. Rev. Lett. **87**, 173001 (2001).
[18] R. Yamazaki and D. S. Elliott, Phys. Rev. Lett. **98**, 053001 (2007).
[19] R. Yamazaki and D. S. Elliott, Phys. Rev. A **76**, 053401 (2007).
[20] N. L. Manakov, V. D. Ovsiannikov, and A. F. Starace, Phys. Rev. Lett. **82**, 4791 (1999).
[21] A. Bolovinos, S. Cohen, and I. Liontos, Phys. Rev. A **77**, 023413 (2008).
[22] N. B. Baranova, B. Ya. Zel'dovich, A. N. Chudinov, and A. A. Shul'ginov, Zh. Eksp. Teor. Fiz. **98**, 1857 (1990) [Sov. Phys. JETP **71**, 1043 (1990)].
[23] N. B. Baranova and B. Ya. Zel'dovich, J. Opt. Soc. Am. B **8**, 27 (1991).
[24] L.-Y. Peng and A. F. Starace, Phys. Rev. A **76**, 043401 (2007).
[25] Y.-Y. Yin, D. S. Elliott, R. Shehadeh, and E. R. Grant, Chem. Phys. Lett. **241**, 591 (1995).
[26] G. Laplanche, M. Jaouen, and A. Rachman, J. Phys. B **19**, 79 (1986).
[27] A. N. Grum-Grzhimailo, A. D. Kondorskiy, and K. Bartschat, J. Phys. B **39**, 4659 (2006).
[28] See https://www.tacc.utexas.edu/stampede.
[29] A. N. Grum-Grzhimailo, B. Abeln, K. Bartschat, D. Weflen, and T. Urness, Phys. Rev. A **81**, 043408 (2010).
[30] A. N. Grum-Grzhimailo, M. N. Khaerdinov, and K. Bartschat, Phys. Rev. A **88**, 055401 (2013).
[31] I. A. Ivanov, A. S. Kheifets, K. Bartschat, J. Emmons, S. M. Buczek, E. V. Gryzlova, and A. N. Grum-Grzhimailo, Phys. Rev. A **90**, 043401 (2014).
[32] V. V. Balashov, N. M. Kabachnik, and A. N. Grum-Grzhimailo, *Correlation and Polarization Phenomena in Atomic Collisions* (Kluwer Academic/Plenum Publishers, New York, 2000).
[33] B. Gao and A. F. Starace, Phys. Rev. Lett. **61**, 404 (1988).
[34] B. Gao and A. F. Starace, Phys. Rev. A **39**, 4550 (1989).
[35] A. E. Orel and T. N. Rescigno, Chem. Phys. Lett. **146**, 434 (1988).
[36] A. A. Krylovetsky, N. L. Manakov, and S. I. Marmo, JETP **92**, 37 (2001).
[37] H. B. Bebb and A. Gold, Phys. Rev. **143**, 1 (1966).
[38] A. T. Georges and P. Lambropoulos, in *Advances in Electronics and Electron Physics*, edited by L. Marton and C. Marton, Vol. 54 (Academic Press, New York, 1980), p. 191.
[39] T. Nakajima, Phys. Rev. A **61**, 041403(R) (2000).
[40] H. Kleinpoppen, B. Lohmann, and A. N. Grum-Grzhimailo, *Perfect/Complete Scattering Experiments* (Springer, New York, 2013).